https://doi.org/10.5194/nhess-2023-120
Preprint. Discussion started: 8 August 2023

Natural Hazards and Earth System Sciences
Discussions

Predictive Understanding of Socioeconomic Flood Impact in Data-Scarce Regions Based on Channel Properties and Storm Characteristics: Application in High Mountain Asia (HMA)

Mariam Khanam[1], Giulia Sofia[1], Wilmalis Rodriguez[1], Efthymios I. Nikolopoulos[2], Binghao Lu[3], Dongjin Song[3] and Emmanouil N. Anagnostou[1]

[1]Civil & Environmental Engineering, University of Connecticut, Storrs, 06269, USA
[2]Civil & Environmental Engineering, Rutgers University, Piscataway, 08854, USA
[3]Computer Science and Engineering, University of Connecticut, Storrs, 06269, USA

Correspondence to: Mariam Khanam (mariam.khanam@uconn.edu), Giulia Sofia (giulia.sofia@uconn.edu)

Abstract. The exposure of High Mountain Asia (HMA) to disaster risks is heightened by extreme weather conditions and the impacts of climate change. Obtaining knowledge about the long-term response of the landscape to hydroclimatic variations in HMA is paramount, as millions of people are affected by these changes every year. During monsoons, substantial human suffering, and damage to crops and infrastructure in populated communities result from the flooding and debris flow caused by the increase in precipitation extremes each year. Although a few initiatives have undertaken the estimation of flood risk locally, the use of traditional techniques in ungauged basins is, unfortunately, not always possible because of the lack of extensive data required. To address this problem, we present in this study a geomorphologically guided machine learning (ML) approach for mapping flood impacts across HMA. We defined socioeconomic flood impact using the Lifeyears Index (LYI), a systematic index that measures the economic cost and loss of life caused by flooding. This index quantifies the importance of the destruction to infrastructure, capital, and housing in an overall assessment. We trained the proposed model with over 6000 flood events, from 1980 to 2020, and their computed five-year and ten-year LYIs. We used as predictors, (1) the five-year rainfall concentrations (which correlate the magnitude of precipitation events with the time of occurrence) of events retrieved from ERA5 daily data; (2) a geomorphic classifier (flood geomorphic potential) based on hydraulic scaling functions automatically derived from an 8 and 30-meter digital elevation model (DEM) for the region and (3) population. This model proved capable of identifying the hotspots of flood susceptibility on a national scale and showing its variability from 1980 to 2022. The study also highlights the severity of the impacts of hydroclimatic extremes in the entire HMA region. The framework is generic and can be used to derive a wide variety of flood vulnerability and subsequent risk maps in data-scarce regions.

1 Introduction

High Mountain Asia (HMA) has a highly complex terrain with active hydrologic and geomorphologic processes. The region has experienced the effects of climate change, including expedited glacial melt (Shrestha and Aryal, 2011; Byers et al.,

https://doi.org/10.5194/nhess-2023-120
Preprint. Discussion started: 8 August 2023


Natural Hazards and Earth System Sciences Discussions

2022) and altered precipitation intensity (Haag et al., 2019; Kirschbaum et al., 2020). These changes, combined with other anthropogenic and environmental factors (such as population growth and landscape modifications), have increased the likelihood of flooding(Byers et al., 2022; Pervin et al., 2020; Shrestha et al., 2010; G. Zheng et al., 2021), which is now a grave threat to life, agriculture, and infrastructure in the region (Fischer et al., n.d.; Pervin et al., 2020; Rentschler et al., 2022; Sharma et al., 2019; Torti, 2012). The direct impacts caused by the flood waters are further exacerbated by the significant long-lasting socioeconomic consequences of floods, including losses of livelihood, need for rehabilitation, and psychological harm.

Flood disasters are generally associated with hydroclimatic extremes. The variability of precipitation patterns over time, space, and intensity is indeed crucial to their occurrence, but changes in catchment characteristics can also alter flood magnitude and frequency. The complex geomorphology and orographic characteristics in the HMA region cause significant spatiotemporal heterogeneity of precipitation patterns and extremes (Haag et al., 2019). Furthermore, the geomorphic structure of basins in HMA can influence the flood characteristics more than landcover does (Marston et al., 1996). Many floods in HMA carry huge amounts of sediment and water that adversely affect downstream areas with large human populations and can remain in the landscape for years afterward (Kafle et al., 2017; Simonovic et al., 2022).

Changes in river morphology and channel shifting resulting from sediment variability are recognized causes of flood risk (Blench, 1969; Criss & Shock, 2001; Lane et al., 2007; Neuhold et al., 2009; Pinter et al., 2008; Slater et al., 2015; Stover & Montgomery, 2001). Several researchers have highlighted how the morphometric characteristics of watersheds provides useful insights into their hydrologic response to rainfall (Borga et al., 2008) since their morphometric characteristics are a crucial influence on flash flood intensity. In HMA, however, these control mechanisms are difficult to model at the large scale.

To date, available studies (Diehl et al., 2021; Mohanty & Simonovic, 2022; Pangali Sharma et al., 2019; Pervin et al., 2020; Piacentini et al., 2020; Yang & Tsai, 2000) have focused on vulnerability mapping and risk analysis carried out through case studies and descriptive methods on a local scale. Flood vulnerability studies conventionally use hydrologic or hydrodynamic simulations, which require large amounts of time and data. Although improved rainfall-runoff simulations can make flood mapping more accurate, HMA does not have enough hydrological stations for region-wide flood monitoring. Moreover, the available meteorological datasets may not be sufficiently trustworthy. Accurate flood modeling is challenged by the inadequate spatial coverage of hydrological observations, which introduces uncertainty in forecasting, and flood risk management, and reduces the ability to mitigate disaster impacts through planning and management. Besides traditional flood hazard mapping, accurate evaluation of socioeconomic impacts of natural disasters (Cavallo & Noy, 2010; Meyer et al., 2013; Noy, 2015, 2016a) is foremost to mitigate the sufferings of the affected people and rehabilitation(Cavallo & Noy, 2010; Meyer et al., 2013; Noy, 2015, 2016a).

Geomorphic properties, population data, and rainfall characteristics are rarely investigated together on a large scale as a means of measuring socioeconomic flood impact. The use of remote sensing technology for disaster studies in HMA is comparatively new and can benefit from modern, improved-resolution datasets. During the past few decades, empirical studies (Diehl et al., 2021; Jongejan & Maaskant, 2015; Mosavi et al., 2018) on flood vulnerability mapping have proliferated drastically, facilitated by the increased availability of high-resolution global datasets (Bentivoglio et al., n.d.; Diehl et al., 2021;

https://doi.org/10.5194/nhess-2023-120
Preprint. Discussion started: 8 August 2023


Natural Hazards and Earth System Sciences Discussions

Dottori et al., 2022; Hawker et al., 2018; Kirschbaum et al., 2020; Mohanty & Simonovic, 2022; Pangali Sharma et al., 2019; Sanyal & Lu, 2004; Yang & Tsai, 2000; X. Zheng et al., 2018). Additionally, machine learning (ML) techniques have gained popularity in advanced prediction systems over the past two decades, offering more affordable solutions with aggregable performance than simulating the intricate time-demanding mathematical expressions of the physical processes of floods.

Recent studies (Bentivoglio et al., n.d.; Deroliya et al., 2022; Mosavi et al., 2018) have presented promising results in combining ML techniques with global datasets. This modern approach to mapping flood vulnerability significantly reduces the computational times associated with data-demanding simulations. Furthermore, in data-scarce and vulnerable regions, results produced so rapidly and efficiently are very helpful for flood risk management. In ML, however, the system learns based on existing data. The learning is inadequate if the data is insufficient or does not cover all possible variations of the task and, as a result, cannot perform well when put to work. Consequently, rigorous data enrichment in terms of both data quantity and quality is essential. In this study, we present a simplified procedure for preliminary flood vulnerability characterization on a large scale, based on available global datasets. Specifically, we demonstrate a flood-risk assessment model that quantifies spatially distributed socioeconomic susceptibility in flood-prone areas and use the model to improve disaster understanding using remotely sensed data, such as climate variables and high-resolution terrain. Lastly, we apply this model in the data-scarce regions of HMA to understand the changes in socioeconomic flood impacts from 1980 to 2020.

2 Materials and Methods

2.1 Study Area

HMA, otherwise known as the Hindu Kush-Himalayan region, comprises Nepal, Pakistan, Bangladesh, Bhutan, India, Afghanistan, Kazakhstan, Kyrgyzstan, Tajikistan, Uzbekistan, Mongolia, and China. HMA is home to some of the world's highest mountain systems, including the Himalayas and the Hindu Kush. This rugged terrain has a highly variable climate ranging from tropical to subpolar, essentially controlled by altitude. Around 210 million people dwelling in the region are at risk of natural disasters (such as heavy rainfall, flooding (pluvial/ fluvial/ flash), earthquakes, avalanches, and landslides) due to the topographic characteristics, changing climate patterns, and high population density. Some of the world's largest rivers and deltas, such as the Indus and the Ganges reside in this region. In the summertime (June to September), monsoon rains bring a vast amount of water (Kayastha & Kayastha, 2019) to the rivers and valleys in the southern part of HMA (Northern India, Nepal, Bangladesh, and Pakistan). Kirschbaum et al., 2020 have projected that the greatest increase in very high intensities of precipitation (>20 mm/day) will occur during the monsoon season with the enormous amount of rain causing all types of devastating floods (Talchabhadel et al., 2018). Among all other hydroclimatic disasters in HMA from 1980 to 2020 (EMDAT, www.emdat.be), floods affected the most people and caused the most total damage. Bangladesh, Nepal, Pakistan, and parts of India were hotspots with the highest casualties.

In this study, we have taken approximately 6000 watersheds across HMAT into account as our main target area (Figure 1). The analysis initially focused on training and testing the model for Nepal, for which we gathered fine-resolution

https://doi.org/10.5194/nhess-2023-120
Preprint. Discussion started: 8 August 2023

Natural Hazards and Earth System Sciences
Discussions

topographic information and district-scale socioeconomic data related to population characteristics and reported flood impacts. Later, we used the trained model to predict the socioeconomic impacts for all the watersheds across HMA.

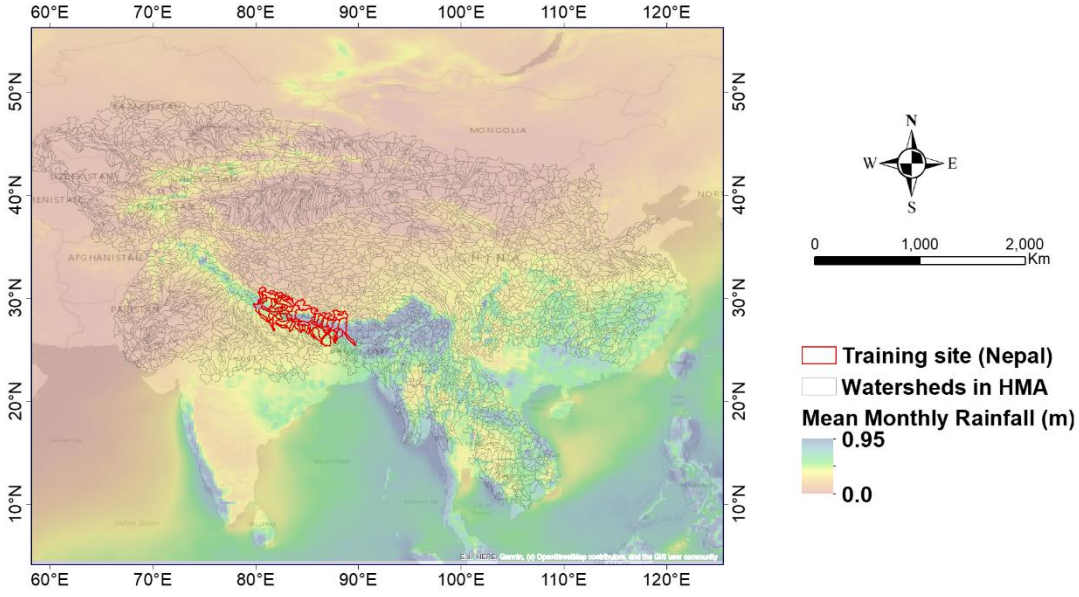

Figure 1: Study area- watersheds across High Mountain Asia (HMA)

2.2 Methods

Figure 2 shows the conceptual framework for the study. We have implemented ML analysis leveraging climatic and geomorphologic variables. To represent exposure and socioeconomic impacts, we introduced, respectively, a variable for population and "Lifeyears Index" (LYI) (Noy, 2014, 2016a, 2016b), a unit of measurement used to describe a disaster's impact in terms of the total years of life lost (see section 2.2.1 for details). As indicated above, the framework overall encompassed two scales. First, we built and trained the model using detailed flood damage reports from Nepal. Then we applied the trained model to the whole HMA to predict the socioeconomic impact of the extreme flood events from 1980 to 2020. To predict the LYI, we applied XGBoosting (eXtreme Gradient Boosting) (Chen et al., 2018; Chen & Guestrin, 2016). The predictor and response variables of the ML framework are described in the subsections below.

https://doi.org/10.5194/nhess-2023-120
Preprint. Discussion started: 8 August 2023

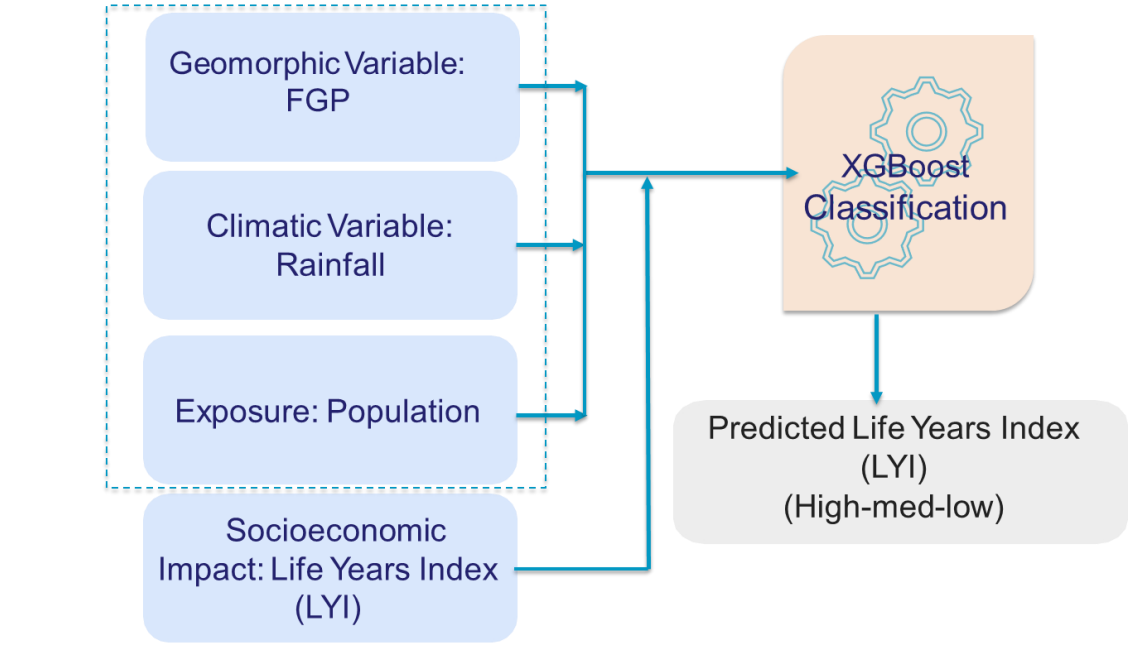

Figure 2: Conceptual framework. Considered predictors are Flood Geomorphic Potential (FGP), Rainfall, and Population. The predicted value is the socioeconomic impact, characterized as Lifeyears Index (LYI) (Noy, 2016a; Noy, 2015). Readers should refer to section 2.2.1, 222 …. for an explanation of the predictors and predicted values.

2.2.1. Socioeconomic Flood Impacts

The research focused on predicting the socioeconomic impact of floods. Measured economic loss and tangible damages were analyzed by considering the Lifeyears Index (LYI) (Noy, 2014, 2016a, 2016b). This index is presented by Noy, 2016 as "Lifeyears lost" modified from Disability Adjusted Life Years (DALYs) lost due to diseases and injuries(WHO, 2014) to use for demonstrating disaster. We calculated LYI for Nepal by using damage statistics and demographic information collected from different data portals in Nepal. The index is described by equation 1:

$$LYI = M(Aexp - Amed) + e * T * N + (1 - c)Y/PCGDP \quad (1)$$

where M = Mortality (number of deaths due to disaster, source: https://data.worldbank.org/country/Nepal, https://knoema.com/atlas/Nepal/topics/Demographics/Age/Life-expectancy-at-birth (life expectancy 2020)); Aexp = Average life expectancy at birth (by year) (sources: https://knoema.com/atlas/Nepal/topics/Demographics/Age/Median-age-of-population); Amed = Median age (by year); e = Welfare reduction weight associated with being exposed to a disaster (set to e = 0.054 according to Noy, 2016a, based on Mathers et al., 2013; T = Time taken by the affected person to get back to normal (following the suggestions of Noy, (2016a) we set this to T = 3yrs, which after being multiplied by "e" amounts to about 59 days/person); N = Number of affected people(source: http://drrportal.gov.np/); c = Percent of time not used in work-related activities (.75); Y = Financial damage (value of destroyed/damaged infrastructure) (source: http://drrportal.gov.np/); and

https://doi.org/10.5194/nhess-2023-120
Preprint. Discussion started: 8 August 2023


Natural Hazards and Earth System Sciences
Discussions

PCGDP = Income per capita (by year). We used PCGDP as an indicator of the cost of human effort but discounted this measure by 75 percent (c) in our benchmark calculations to account for the observation that people spend much of their time engaged in activities unrelated to work (Noy, 2016a).

For this study, we categorized the LYI values into three classes: Low when log(LYI) < 2; Med when log(LYI) is between 2 and 3; and High when log(LYI) > 3. This classification implied that a watershed or district is considered at high risk if the average LYI for the basin or district is over 1000 years. Medium is between 100 and 1000 years, and low is less than 100 years. For example, if the calculated LYI is 100 years that means for the given disaster the estimated impact is compared to be as a loss of potential 100 years of life per 100000 people. It is demonstrated by taking into consideration the temporal, financial, physical, and mental effects it has on people.

The cumulative LYI for Nepal (Figure 3) can provide an idea of how the cumulated flood impact has been increasing in that country with time. It also highlights how the index itself captures major disasters, such as those occurring in 1981 (ICIMOD, 2011; Kiran S et al., 2008), 1993 (Nepal - Floods and Landslides, 1993), in 1996 (Nepal - Floods Situation Report No. 1, 26 July 1996), and in the monsoon seasons in 2003 and 2014 (Nepal Annual Report, 2003.; Nepal: Landslides and Floods - Aug 2014). The most changes can be noticed in the LYI for the years 1981, 1993, and 2014, the cumulative step change for these years from the previous year are subsequently 9999, 82865, and 976238 years.

https://doi.org/10.5194/nhess-2023-120
Preprint. Discussion started: 8 August 2023

Natural Hazards and Earth System Sciences
Discussions

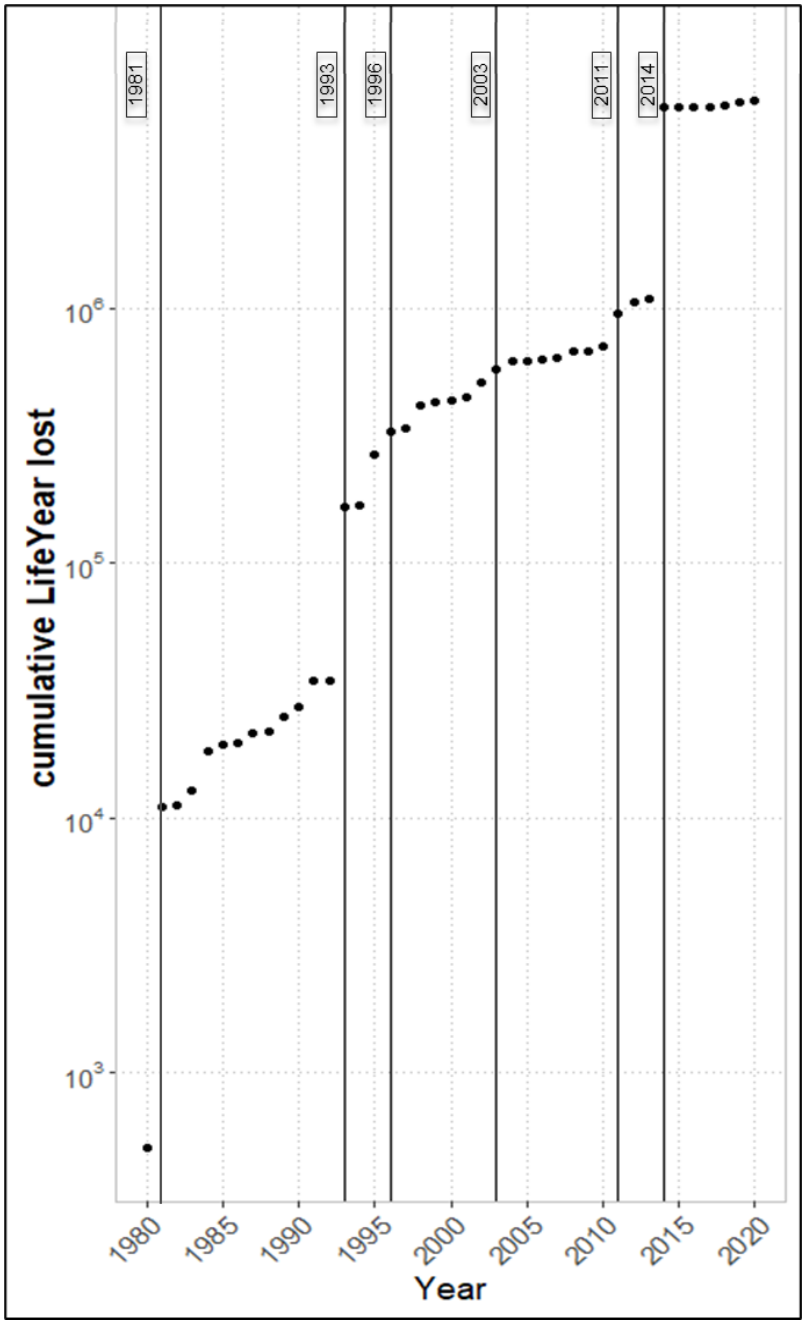

Figure 3: Cumulative lifeyears lost over the years in Nepal. Highlighted years represent jumps in the cumulative value, mostly related to well-known disasters): 1981 (ICIMOD, 2011; Kiran S et al., 2008)**, 1993** (Nepal - Floods and Landslides, 1993)**, 1996** (Nepal - Floods Situation Report No. 1, 26 July 1996)**, and in the monsoon seasons in 2003 and 2014** (Nepal Annual Report, 2003.; Nepal: Landslides and Floods - Aug 2014).

https://doi.org/10.5194/nhess-2023-120
Preprint. Discussion started: 8 August 2023


Natural Hazards and Earth System Sciences
Discussions

2.2.2. Floodplain Mapping

The identification of areas with the potential to be inundated is fundamental to preserving and protecting human lives and property while safely supporting economic activities. Hence, we applied a large-scale floodplain delineation algorithm to identify such areas at the basin scale across the HMA. Many researchers (e.g., Dingle et al., 2020; Lindersson et al., 2021; Piacentini et al., 2020) have used DEM-derived geomorphic index as a high-resolution flood mapping tool. We defined our Flood Geomorphic Potential (FGP) index as the logarithm of the ratio between the bankfull elevations (estimated using a hydraulic scaling function, or HSF, based on contributing area) in the element of the river network closest to the point under examination and the elevation difference between these two points (Figure 4). This index was originally defined by Samela et al., 2017, as the Geomorphic Flood Index (GFI), but we improved upon it in one main aspect: for the definition of the HSF, we focused the FGP on the analysis of river widths rather than river depths because, unlike with river depth or velocity, the measurement of river width through remote sensing is straightforward (Sofia et al., 2015; Sofia, et al., 2017a; Sofia & Nikolopoulos, 2020). To this end, we implemented a way to retrieve bankfull width automatically through the landscape (Sofia, et al., 2017b; Sofia et al., 2015). The advantage of its implementation is that FGP is automated and does not require any additional information other than terrain data.

For this analysis, we trained the model considering FGP derived from the unique 8-meter Digital Elevation Models (DEMs) for Nepal that are available at the NASA National Snow and Ice Data Center Distributed Active Archive Center (NSIDC DAAC) (Shean, 2017c, 2017b, 2017a). While Nepal is entirely covered by the 8m DEM, extending the model to the whole HMA region is complicated by the gaps in the input satellite strip resulting from limited coverage, clouds, or failed stereo correlation. For this reason, we also considered the 30m DEM by Copernicus (European Space Agency, Sinergise. Copernicus Global Digital Elevation Model, 2021), a digital surface model (DSM) that represents the surface of the Earth, including buildings, infrastructure, and vegetation. Importantly, this DSM is derived from World DEM, an edited DSM in which the flattening of water bodies and the consistent flow of rivers have been included. Shore- and coastlines, special features such as airports, and implausible terrain structures have also been edited.

We identified flood-prone areas by grouping them into six classes by their FGP index. For each watershed, we then considered the areas covered by the classes with FGP greater than 4, which, when compared to published data, proved to correspond realistically with areas subject to floods of about 100-year depth. Figure 4b shows an example of the FGP automatic classes derived for some rivers in Nepal, compared to baseline scenarios fromDelalay et al., 2018 of inundation extent based on water depth. The comparison confirmed that the modified topographic index was a useful and rapid tool for delineating flood-prone areas in ungauged basins and in areas where expensive and time-consuming hydrologic-hydraulic simulations were not possible.

https://doi.org/10.5194/nhess-2023-120
Preprint. Discussion started: 8 August 2023

Natural Hazards and Earth System Sciences
Discussions

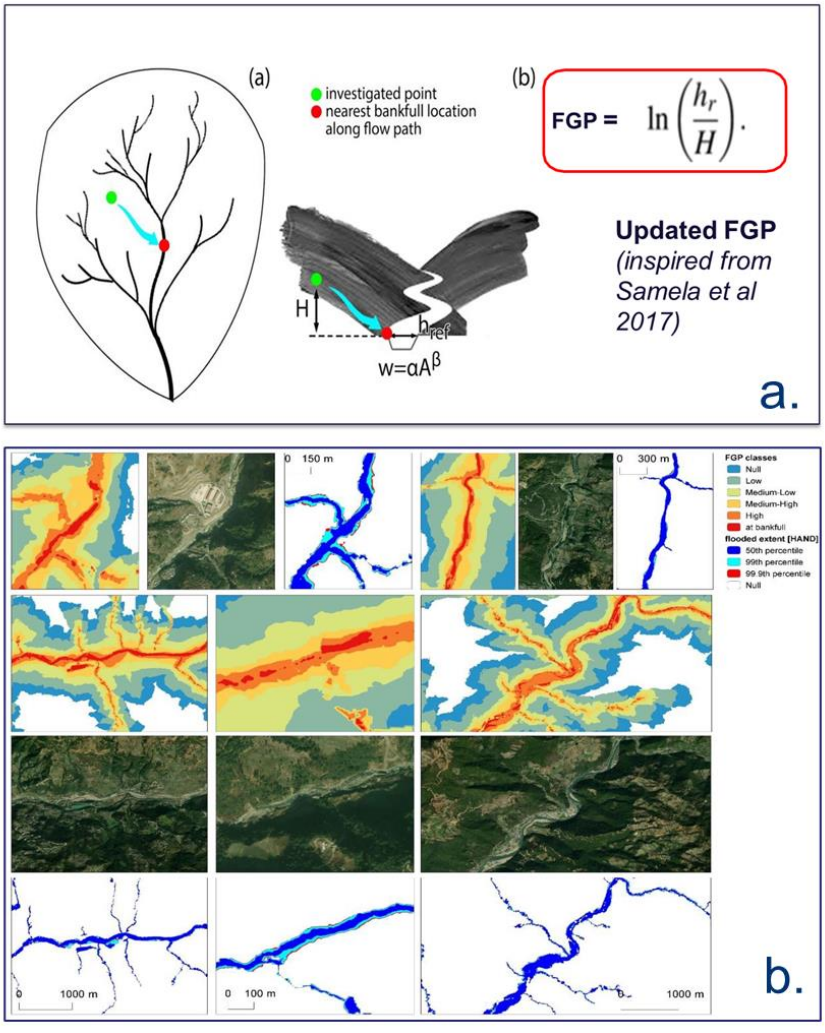

Figure 4: a. Flood Geomorphic Potential (FGP) (modified from Samela et al. 2017); b. FGP automatic classes compared to baseline inundation depth scenarios (aerial imagery by © Google Earth 2015).

2.2.3. Rainfall Characteristic

As rainfall is the main driver of fluvial flooding, we decided to focus on a specific aspect of precipitation: its daily concentration. Sofia et al., (2017) have highlighted how this parameter can capture the dynamics of flood impacts in time. Different authors have adopted different methods to determine the temporal concentration of precipitation, and the Concentration Index (CI) (Equation 2) is one of the most used parameters (Caloiero et al., 2019; Martin-Vide, 2004; Monjo, 2016; Sangüesa et al., 2018; Serrano-Notivoli et al., 2018).

This index was proposed by Martin-Vide (2004) originally to explore the contribution of the days with major rainfall to the total amount within a certain time range. The benefit of this index is that it can describe the temporal variability of

https://doi.org/10.5194/nhess-2023-120
Preprint. Discussion started: 8 August 2023

Natural Hazards and Earth System Sciences
Discussions

rainfall at daily, annual, and seasonal scales using a single metric, as well as spatial variability at pixel or watershed scale; which is an advantage for data-scarce regions.

In the present study, we computed CI (modified from Martin-Vide, 2004) using the ERA5 hourly rainfall data from 1980 to 2019. We identified storm events from this dataset primarily based on the criterion of rainfall of more than 0.5 mm for less than 12 hours. Furthermore, we calculated CI using the cumulative amount of rainfall (y) and the cumulative frequency of the event duration (x) (Figure 5) for the selected events. The method (similar to Cortesi et al., 2012 and Monjo & Martin-Vide, 2016a) eventually aggregates the amount of precipitation that falls during each event into increasing categories and determines the relative contribution (as a percentage) of the progressively accumulated precipitation, y, as a function of the accumulated percentage of the durations of the events (x). The concentration index is then calculated as the ratio of the area between the line of equality (y=x) and the fitted curve (S), and the total area under the line of equality (A+S) (Figure 5, equation 2). The index is defined by the relationship between the accumulated percentage of time, and the accumulated rainfall.

$$CI = \frac{S}{S+A} \quad (2)$$

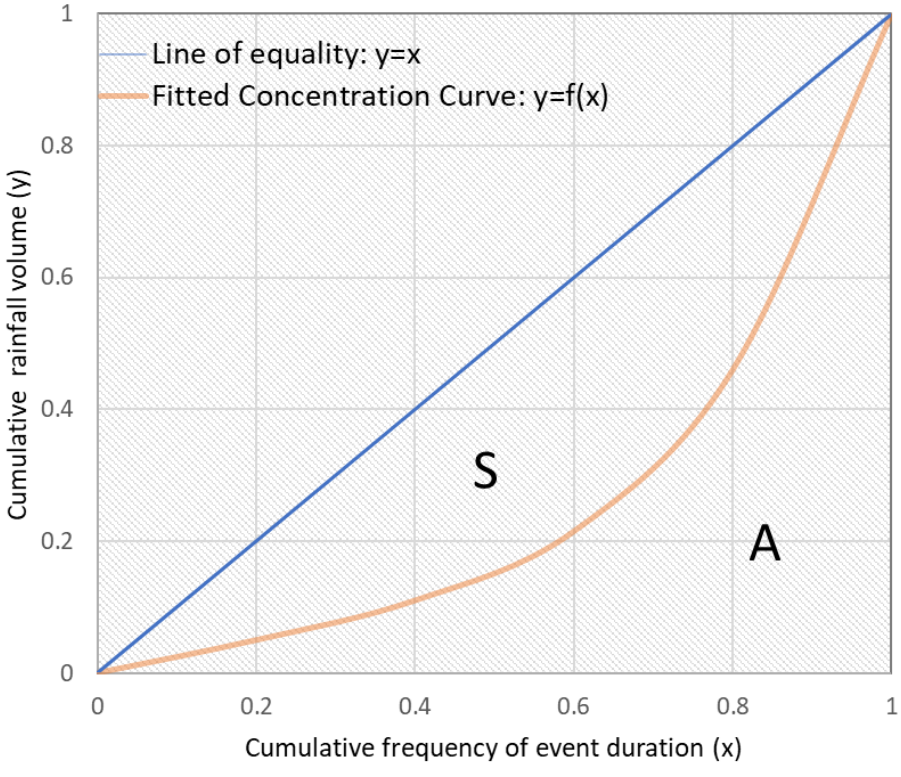

Figure 5: Example of line of equality, and empirical curve for the rainfall concentration calculation. The concentration index is equal to the area between the line of equality and the fitted curve (S) divided by the total area below the line of equality (S+A)

https://doi.org/10.5194/nhess-2023-120
Preprint. Discussion started: 8 August 2023


Natural Hazards and Earth System Sciences
Discussions

2.2.4. Exposure (Population)

As all the parameters of the LYI are not always readily available, we added population counts as one of the predictors to train the model. For Nepal, we selected the data from the country's national census (https://censusnepal.cbs.gov.np/Home/Index/EN). To extend the model to the whole HMA, we computed the population for each watershed across the region from the GHSL: Global Human Settlement Layers, Population Grid 1975-1990-2000-2015. This dataset depicts the distribution and density of the population, expressed as the number of people per cell, for reference epochs. We used a simple linear regression to retrieve data for the missing years.

2.3. Machine Learning Model

While XGBoosting is primarily used to solve classification problems. To generate the results, the XGBoost algorithm uses an ensemble of boosted trees. An ensemble is a collection of predictors that together can give a final prediction while reducing errors significantly. In this case, the predictors were climatic variables, geomorphologic variables, and exposure. Boosted algorithms are those in which each successive model attempts to correct the errors of its predecessor (similar to adaptive learning). The basic XGBoost algorithm can be understood as an ensemble of boosted trees. The idea behind such an ensemble is that multiple trees are built in sequence, each tree built on the previous one's prediction. And each successive tree built considers the errors of the previous trees. This means that when we take an average of all the trees at the end, we get a final tree that is better than any individual tree within the model. We applied the XGBoosting model to the geomorphologic, climatic, and exposure variables to predict classes of LYI in different basins in Nepal and HMA.

2.3.1. Variable Importance and Model Performance

Based on the methodology described in section 2.3, in this section, we present a variable importance comparison (Figure 6) based on the F score. The initial variable importance indicated that population (Pop) was the most important variable, which was consistent with our expectation in the sense that the socioeconomic impact depends entirely on the exposure. The climate variable (CI) happened to be the next important variable, showing the significance of the region's climate on the socioeconomic impact of flood occurrences.

The precision, recall, and F1 score are metrics used to evaluate the performance of a classification model. Precision is the fraction of true positives among the predicted positives. Recall is the fraction of true positives among the actual positives. F1 score is the harmonic mean of precision and recall.

The evaluation metrics reveal in Table 1 that the model performs best in the High class, with the highest precision, recall, and F1 score. The Medium class also demonstrates relatively high performance across these metrics. However, the Low class exhibits the lowest performance, suggesting that the model may face challenges in accurately distinguishing between the Low and Medium classes or may demonstrate a bias toward predicting the Medium and High classes. These findings provide

https://doi.org/10.5194/nhess-2023-120
Preprint. Discussion started: 8 August 2023

Natural Hazards and Earth System Sciences
Discussions

valuable insights into the strengths and limitations of the classification model and can guide future efforts to improve its performance.

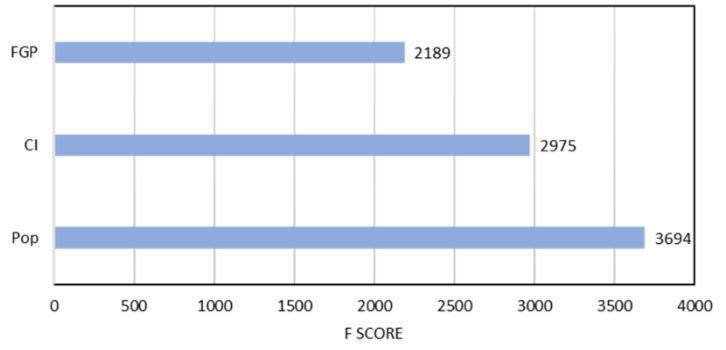

Figure 6: Feature Importance

Table 1: Performance metrics of a classification model

	precision	**recall**	**f1-score**
Low	0.54	0.57	0.56
Medium	0.64	0.63	0.64
High	0.73	0.71	0.72

2.3.2 Validation of the System at the HMA Scale

We tested and validated the model over Nepal, using the calculated LYI data for the region. When extending its applicability to the whole HMA, we evaluated the quality of our result by comparing the predicted social impact with that of existing floods over the region. To ascertain the latter, we compared the results of our mapping to the Dartmouth Flood Observatory's (DFO) Global Active Archive of Large Flood Events, 1985–Present (Brakenridge, n.d.), which contains information on major floods derived from news, governmental, instrumental, and remote sensing sources. The dataset reports multiple pieces of information for each flood, including its meteorological and climatological severity.

Meteorological and climatological severity cannot directly capture the social impact of the floods; furthermore, it refers to an event, which may span multiple watersheds. To overcome these limitations, we compared our predicted results to the DFO data by evaluating a proxy of the social severity reported for each flood—the numbers of "Deaths" and "Displaced" that resulted—rather than the flood's meteorological characteristics. We then considered classes of DFO "social severity" of 10^n. Here n is the severity level declared in the DFO database. Next, we calculated the marginal probability that events with

https://doi.org/10.5194/nhess-2023-120
Preprint. Discussion started: 8 August 2023


Natural Hazards and Earth System Sciences Discussions

different severity in the DFO happened in watersheds with different predicted LYIs. Finally, we calculated the conditional probability, as in the probability of an event of DFO severity of some kind occurring over watersheds where our LYI prediction was of a certain type. This conditional probability could provide us with information on how our system performed for different time frames—for example, the probability of a watershed's being classified as high impact by our model might be only 10% of the total, but if most of DFO events with great severity (i.e., >1000 Deaths+displaced) did happen in those watersheds, then our system correctly identified the risk there.

3. Results Analysis

3.1. Variability of the Predictors

The topographical characteristics of an area can influence the local climate and population distribution. Figure 7 shows an example of how climate concentration and population vary in HMA, as compared to watersheds that have areas of high FGP of greater or lesser extent. The figure reports the average for the time frame 1980–2020 for CI and population, while the FGP is a static value for the time frame (since it is based on a unique DEM dataset), and it represents the overall geomorphic characteristics of Nepal.

From this analysis, we can see how the variability of CI is complex and related to atmospheric characteristics (Sangüesa et al., 2018) as well as geographical factors (Tuladhar et al., 2020), as represented by the classes of FGP. In their study based on Nepal, Karki et al., 2017highlighted the difference in the spatial pattern of high-intensity storm events from that of annual and monsoon events. The rapid rate at which physical processes (e.g., convection) take place regulates the high temporal concentration of precipitation in the regions where the sea surface and ground are highly affected by warmer temperatures (Monjo & Martin-Vide, 2016b). On the other hand, the low temporal concentration of rainfall is characterized as a normal pattern caused by cyclical weather events (Monjo & Martin-Vide, 2016).Watersheds with lesser floodplain extents (that is, less areas with high FGP) are related to higher and steeper mountains, with complex orography. Research has shown that low areas in Nepal are susceptible to receiving high-intensity storm events even though they have fewer wet days (Karki et al., 2017). The authors of the same study also observed that the low-intensity events (annual and monsoonal precipitation) were mostly predominant over Nepal's western middle mountains and central high mountains. In another study, however, Subba et al., 2019 stated that the frequency of extreme events had decreased significantly over the past two decades in the eastern part of Nepal. This shows how the climate concentration is influenced by the landscape of HMA and further confirms the overall variability we captured and present in Figure 7.

Much of the population of Nepal tends to be concentrated in areas with higher FGP, as is typical for mountainous areas, where population and economic activities are mostly located in the river valleys. Globally, the floodplains of rivers are preferred living spaces for the population and provide favorable locations for economic development. These areas are commonly exposed to floods, however, an increasing population, together with the changes in storminess, mean that the risks from flooding are expected to rise.

https://doi.org/10.5194/nhess-2023-120
Preprint. Discussion started: 8 August 2023

Natural Hazards and Earth System Sciences
Discussions

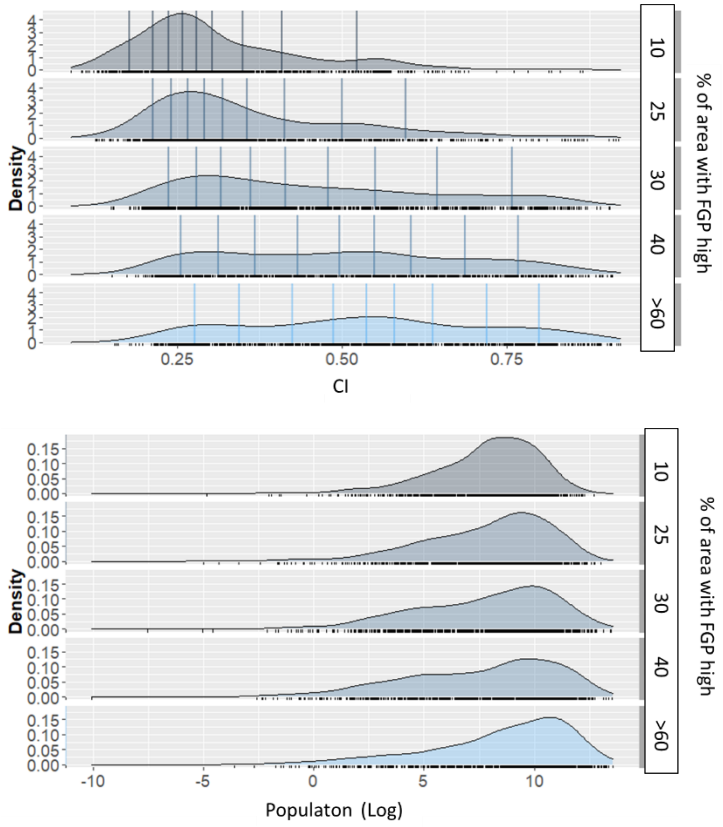

Figure 7: Average variability of the CI (top) and population (bottom) compared to FGP from 1980-2020

3.2. Predicted versus Observed Flood Impact in Nepal

In our comparison of the predicted LYI flood impact with the observed dataset, we found the areas with high-risk levels in Nepal matched well with the locations of historical floods there, suggesting that the proposed method can zone the flood risk on a national scale. Since, for our training site, we had district-level information on the LYI, while geomorphological and hydrological processes happen at the watershed scale, we evaluated the quality of the ML approach at both scales.

Figure 8 demonstrates the comparison between predicted and actual impacts at the watershed (upper row of the figure) and district (lower row) levels. For Nepal, we found the overall training accuracy to be 97% and the test accuracy 63%. The results from training the model at the watershed level were more accurate than those at the district level. This is likely because watersheds are hydrologic units carrying the properties of geomorphology and climate and thus are better connected to the flood than any demographic boundaries—in this case, districts). For the results by watershed, almost all of the year ranges were a 100% match for the actual damage. In the year ranges where the model performed with less than 100% accuracy (i.e.,

https://doi.org/10.5194/nhess-2023-120
Preprint. Discussion started: 8 August 2023

Natural Hazards and Earth System Sciences
Discussions

1985–90 and 1990–95), the LYI in the missed watershed was low, possibly suggesting that the considered predictors were more representative of major flooding.

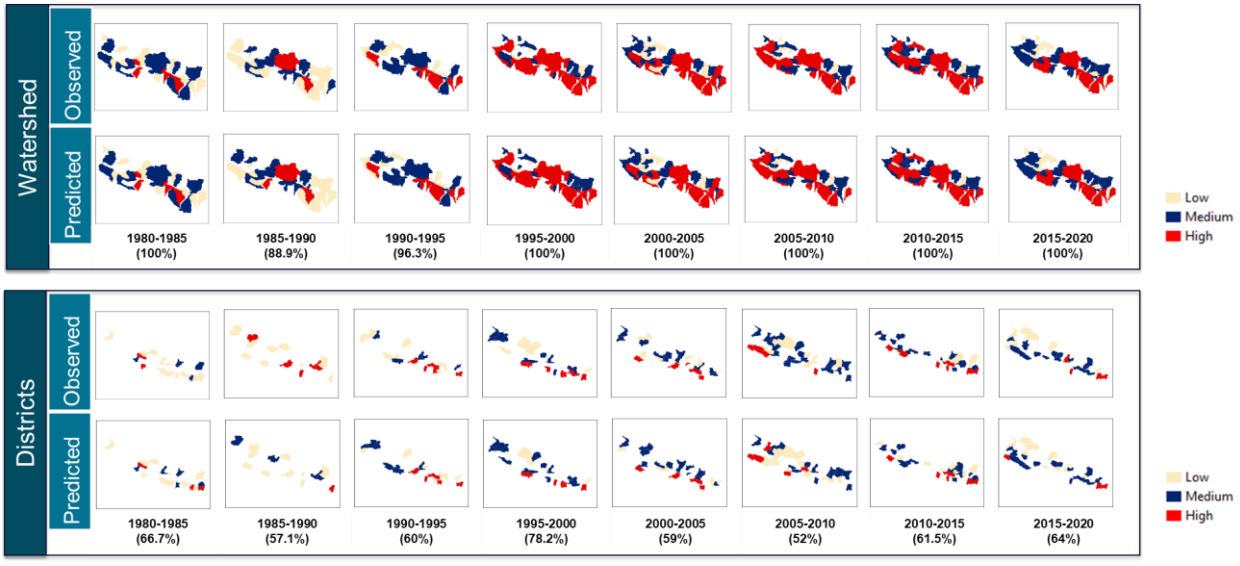

Figure 8: Comparison of prediction with actual socioeconomic impact for watershed on Nepal. Basin/districts are marked as "high" for LYI over 1000 years. Medium is between 100 and 1000, and low is less than 10. Numbers in parentheses represent accuracy.

3.4. Prediction of Socioeconomic Impact of Heavy Rainfall over HMA

We applied the trained model for the watersheds in HMA to five-year intervals from 1980 to 2020. As an example, Figure 9(c, d) shows the predicted basin-averaged LYIs (Low-Med-High) for the watersheds in HMA for two different timelines. The yellow circles highlight the changes in flood impact over the decades.

https://doi.org/10.5194/nhess-2023-120
Preprint. Discussion started: 8 August 2023

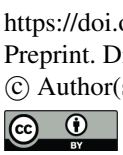

Natural Hazards and Earth System Sciences
Discussions

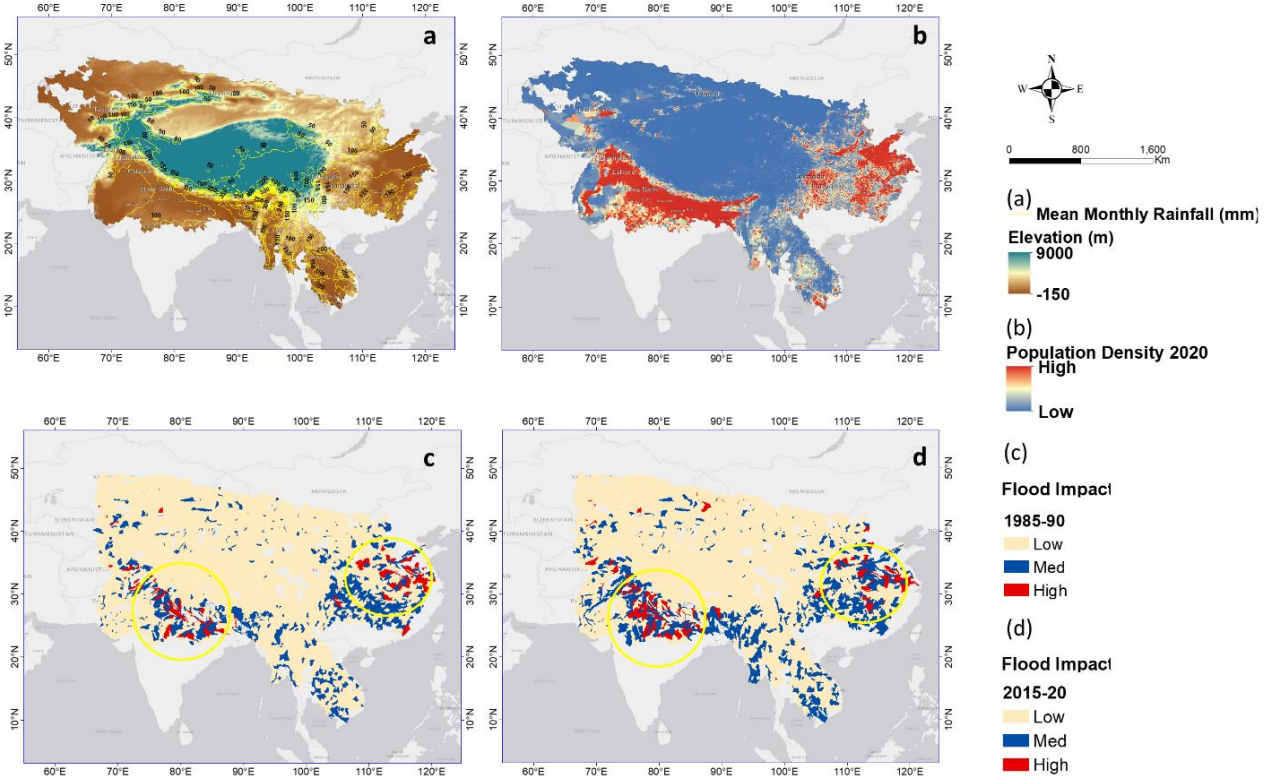

315 **Figure 9: Example of predicted basin-averaged flood impact for HMA (left, 1985–90; right, 2015–20). Yellow circles denote the changes in flood impact between the two timelines.**

Summarizing the results presented in Table 2, we can say that, for the years shown, we predicted almost 57% of watersheds (marginal) having LYIs between 1 and 100 years (Low), 35.9% for LYIs between 100 and 1000 years (Med), and 320 only 6% for LYIs greater than 1000 years (High). For the entire time frame, most of the time we predicted LYIs of 1 to 100 years, for which we captured events of DFO severity around 2 (10^2 Deaths+displaced) (conditional = 28.6%). This suggests that most "Low" class DFO events did happen in the watersheds within the lowest predicted LYI range. Readers must consider that "Low" in this case means the flood impact can range from 1 to 100 years lost, and a DFO value of 2 means total Deaths+displaced is on the order of 10^2 people. The events with a DFO value of 4 happened mostly in watersheds with 325 predicted LYIs ranging both between 1 and 100 years and between 100 and 1000 years. The events with DFO 6 and 8 happened mostly in ranges greater than 1000 years and between 100 and 1000 years.

Table 2: LYI compared to DFO flood damage.

DFO	LYI	NO	Prop	Marginal Probability	Conditional Probability
2	1–100yr	54	16.6	58.2	28.6

https://doi.org/10.5194/nhess-2023-120
Preprint. Discussion started: 8 August 2023


Natural Hazards and Earth System Sciences Discussions

2	100–1000yr	26	8.0	35.7	22.4
2	>1000year	5	1.5	6.2	25.0
4	1–100yr	92	28.3	58.2	48.7
4	100–1000yr	45	13.8	35.7	38.8
4	>1000year	5	1.5	6.2	25.0
6	1–100yr	42	12.9	58.2	22.2
6	100–1000yr	44	13.5	35.7	37.9
6	>1000year	8	2.5	6.2	40.0
8	1–100yr	1	0.3	58.2	0.5
8	100–1000yr	1	0.3	35.7	0.9
8	>1000year	2	0.6	6.2	10.0

We further investigated how our predicted LYI behaved when it was related to the total population (Table 3), evaluating, as suggested by (Noy, 2014), the LYI per capita (that is, the number of lifeyears lost per 100k people). As Table 3 shows, we correctly predicted over the years almost 64% of watersheds (marginal) have LYI/100k people less than 1 year (10^0), 24.3% at 10year/100k people (10^1), 11% at 100year/100k people, and 0.6% at 1000years/100k people. We noticed that LYI/100k people reached, at most, 6000 for Nepal (at the country scale) and the study by Noy. 2016a also reported similar values for Nepal for 1987. (Noy, 2016a) reported actual LYI data in the range of LYI > 1000/100k people in South Asia and stated that the higher number of damages in East and South Asia is likely due to wide-scale flooding. This gave assurance of the consistency of our prediction with the actual data available. When looking at LYI/100k people, we found that, for the whole timeframe, most of the floods that registered in the DFO with low severity (DFO = 10^2 Deaths+displaced) happened in watersheds for which the predicted LYIs were between 1 and 100 years (conditional = 29.8%). This confirmed once again that, in most cases, the “low”-risk events did happen in the lowest predicted range (similar to the findings presented in Table 2). As before, while the probability of a watershed’s being labeled as high risk (LYI>1000year/1000k people) by our system was only 6%, the probability of these watersheds having experienced events recorded by the DFO as having a great impact (DFO severity > 6, meaning over 1 million people) rose to 40% and 10%.

Table 3: LYI/100k compared to DFO flood damage.

DFO	LYI	NO	Prop	Marginal Probability	Conditional Probability
0	0	13	3.8	65.0	5.9
0	1	1	0.3	23.5	1.3
0	2	1	0.3	10.9	2.7
2	0	62	18.2	65.0	28.1

https://doi.org/10.5194/nhess-2023-120
Preprint. Discussion started: 8 August 2023


Natural Hazards and Earth System Sciences
Discussions

2	1	13	3.8	23.5	16.3
2	2	9	2.6	10.9	24.3
2	3	1	0.3	0.6	50.0
4	0	97	28.5	65.0	43.9
4	1	34	10.0	23.5	42.5
4	2	10	2.9	10.9	27.0
4	3	1	0.3	0.6	50.0
6	0	47	13.8	65.0	21.3
6	1	32	9.4	23.5	40.0
6	2	15	4.4	10.9	40.5
8	0	2	0.6	65.0	0.9
8	2	2	0.6	10.9	5.4

Figure 10 shows the LYI per 100k people (LYI/100k) evaluated for different time frames for all the locations reported in the DFO database to compare the DFO severity with our predictions. Overall, the DFO and predicted results were quite consistent instead of some minor variability for some scattered areas. When we compared the changes over time, we noticed an increase in vulnerability. As the plot makes evident, the largest changes took place in 1990–95 and 2010–15; the two concentrated areas were Nepal and China. As Figure 2 showed, two big jumps occurred during these timelines for Nepal because of extreme storm-induced flood events. In Figure 3 we have discussed the predominant events that occurred in these timelines. Regarding China, as of June 2010, more than 29 million people had been affected by flooding, with up to 2.37 million evacuated and 195,000 homes destroyed (China: Floods Information Bulletin N° 1 GLIDE N°, 2010).

https://doi.org/10.5194/nhess-2023-120
Preprint. Discussion started: 8 August 2023

Natural Hazards and Earth System Sciences
Discussions

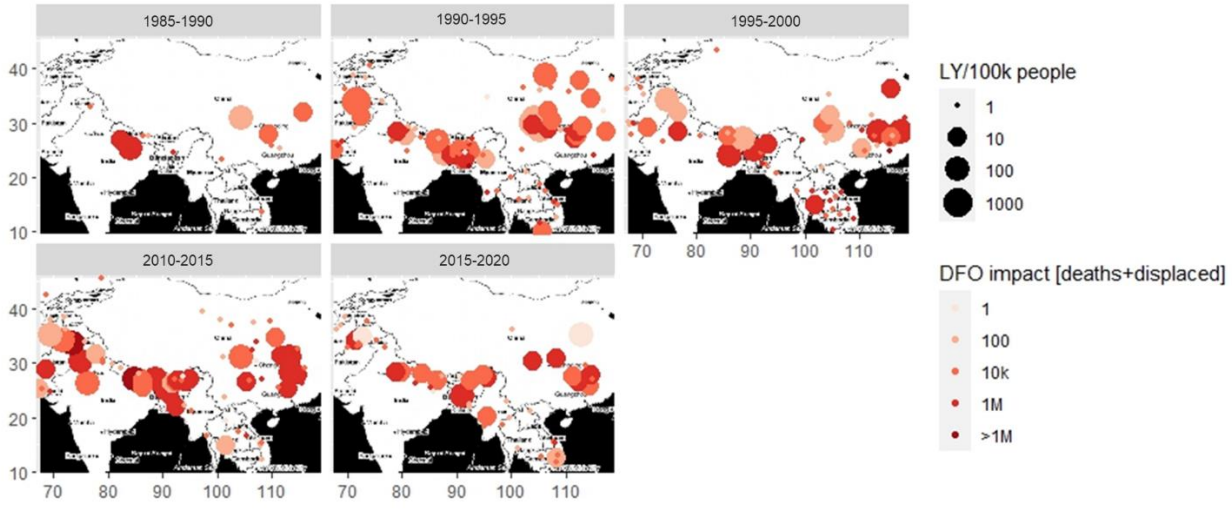

Figure 10: Comparison of DFO and LYI/ 100K people for all the timelines

3.5. Change in Socioeconomic Impact over Time

Figure 11a presents our maps of the watersheds where flood impacts increased over time. Furthermore, Figure 11b shows our evaluation of the percentage changes in the number of watersheds between timelines, focusing on three different changes: low to medium (LtoM); medium to high (MtoH); and low to high (LtoH). The most changes were from LtoM for all the timelines, which represented a notable change in vulnerability. Several watersheds showed higher flood impacts (from low to medium, medium to high, and low to high) in recent years than in 1985–90. Again, we observed the most changes for 1990–95 and 2010–15, which was consistent with Figure 10. The exposure changed significantly, along with the intensity of the events; hence, the risk of flooding was heightened in these areas.

Impact changes from Low to High were next, according to the number of watersheds changed for all the timelines. It was obvious that more changes would happen in the long run, but the comparison of the 1990–95 and 1995–2000 timelines demonstrated that heightened flood impact occurred in a considerable number of watersheds within a short period. For many watersheds, the risk was heightened by a population boom during the overall period.

https://doi.org/10.5194/nhess-2023-120
Preprint. Discussion started: 8 August 2023

Natural Hazards and Earth System Sciences
Discussions

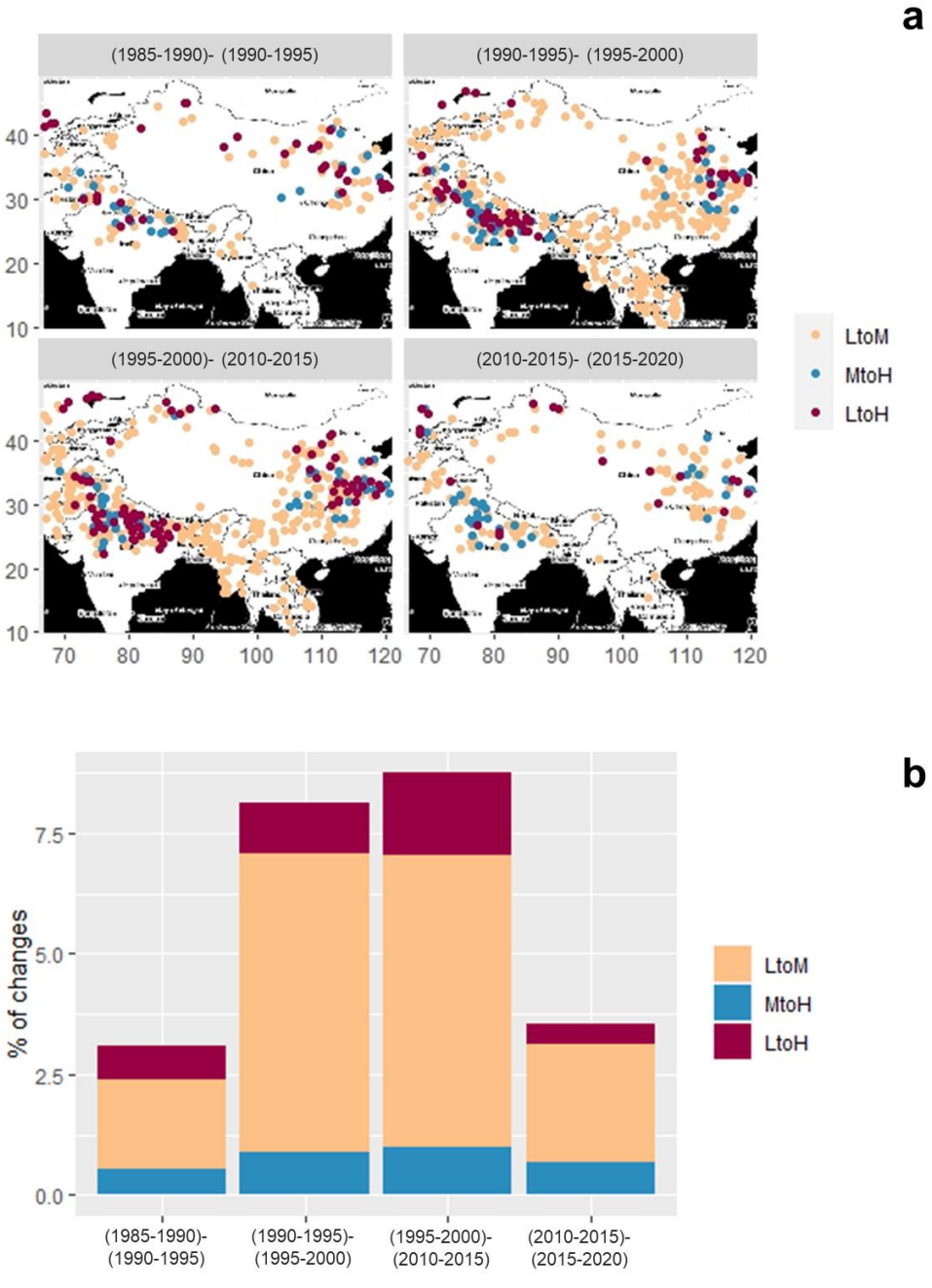

Figure 11: Flood impact change in HMA over time

https://doi.org/10.5194/nhess-2023-120
Preprint. Discussion started: 8 August 2023


Natural Hazards and Earth System Sciences Discussions

4. Conclusions

High Mountain Asia is a complex and diverse region, characterized by its rugged terrain, diverse climate and vegetation, and large population. Disaster management is vital in a data-scarce region like HMA, which is highly vulnerable to natural disasters, and addressing these risks will be vital to ensuring the long-term sustainability of the region and its people. Reducing the significant threat posed by flooding to the population and development of High Mountain Asia requires a multifaceted approach involving investments in disaster risk reduction, sustainable land use practices, and climate change mitigation.

In this study, we demonstrated a simplified approach in which hotspots of vulnerability in the HMA region are identified by intense rainfall events. To map the socioeconomic flood vulnerability of the HMA region, we evaluated a remotely sensed data-driven model that includes both geomorphology and climate variability. The framework can be adapted to different data-scarce regions and allows for integrating possible modifications to flood drivers, including climate variables, geomorphologic variables, and population. The predicted results provide information on vulnerabilities for the different watersheds in HMA, which will enable flood management authorities to plan for a probabilistic mapped area.

The novelty of this study lies in the uniqueness and capability of the model. The predictive model developed in this study demands very few variables to project the socioeconomic impact of future flooding events. In a data-scarce densely populated region and fast-changing climate, such a model can be a great decision-making tool for the end users. The training result for Nepal highlighted the efficiency of the model, and the comparison of results with actual reported flood impacts highlighted how the system can be extended to a larger domain, having comparable morphological and climatic settings, given that we have the availability of terrain data and rainfall information.

Now we have the technology to predict the forcings of an extreme upcoming event, and with this information, we can apply our model to predict the plausible future impact of floods and their severity. In 2022, many provinces of Pakistan were devastated by a series of floods. With close to 2000 deaths, a million homes damaged or destroyed, and a great loss of livestock, this was the most destructive flood event in Pakistan in decades. Our results predicted high vulnerability for certain watersheds in Pakistan for the most recent timeline (2015–20), which was verified in the unseen 2022 event. Stakeholders can utilize our model to predict vulnerability to such future flood events with great accuracy—a development that can provide a better perspective on flood hazards and support decision-making, planning, and investment in mitigation measures.

While the novelty of the study demonstrates the scope for accurate prediction of flood impact in a data-scarce region, the use of static FGP maps has some limitations. Flooding brings a heavy load of sediment to the downstream and floodplains, which alters the channel morphology and affects the prospect of future flooding (Dingle et al., 2020a; Lane et al., 2007; Slater et al., 2015b, 2019; Stover & Montgomery, 2001). Therefore, flood hazards can be underestimated if we omit the “dynamic flood topographies” (Dingle et al., 2020b). Dingle et al., 2020 showed in their study that the inundation extent increases by 9.5% for a moderate flood discharge (20 years) if two DEMS captured 10 years apart are analyzed separately. Although we are aware of this meaningful change in geomorphology, the frequency at which global or local DEMs are acquired is somewhat

constrained. Prediction by our model can be more robust if high-resolution topographical data are available after extreme events.

Competing interests: The contact author has declared that none of the authors has any competing interests.

Acknowledgment: This work was supported by the NASA High Mountain Asia program (grant #80NSSC20K1300).

Data Availability: We are working towards making the FGP products available at NASA National Snow and Ice Data Center (NSIDC)

References

Anon: China: Floods Information bulletin n° 1 GLIDE n°, 2010.

European Space Agency, Sinergise. Copernicus Global Digital Elevation Model: https://doi.org/10.5069/G9028PQB, last access: 20 March 2023.

Nepal - Floods and Landslides Jul 1993 UN DHA Situation Reports 1-8 - Nepal | ReliefWeb: https://reliefweb.int/report/nepal/nepal-floods-and-landslides-jul-1993-un-dha-situation-reports-1-8, last access: 6 February 2023.

Nepal - Floods Situation Report No. 1, 26 July 1996 - Nepal | ReliefWeb: https://reliefweb.int/report/nepal/nepal-floods-situation-report-no-1-26-july-1996, last access: 6 February 2023.

Nepal Appeal No. 01.55/2003 Annual Report - Nepal | ReliefWeb: https://reliefweb.int/report/nepal/nepal-appeal-no-01552003-annual-report, last access: 6 February 2023.

Nepal: Landslides and Floods - Aug 2014 | ReliefWeb: https://reliefweb.int/disaster/ls-2014-000103-npl, last access: 6 February 2023.

Bentivoglio, R., Isufi, E., Nicolaas Jonkman, S., and Taormina, R.: Deep Learning Methods for Flood Mapping: A Review of Existing Applications and Future Research Directions, n.d.

Blench 1906-1993, T.: Mobile-bed fluviology : a regime theory treatment of rivers for engineers and hydrologists, Edmonton (Ca.) : University of Alberta press, 1969.

Borga, M., Gaume, E., Creutin, J. D., and Marchi, L.: Surveying flash floods: Gauging the ungauged extremes, Hydrol Process, 22, 3883–3885, https://doi.org/10.1002/HYP.7111, 2008.

Global Active Archive of Large Flood Events.: https://floodobservatory.colorado.edu/Archives/index.html, last access: 20 March 2023.

Byers, A. C., Shugar, D. H., Chand, M. B., Portocarrero, C., Shrestha, M., Rounce, D. R., and Watanabe, T.: Three Recent and Lesser-Known Glacier-Related Flood Mechanisms in High Mountain Environments, Mt Res Dev, 42, A12–A22, https://doi.org/10.1659/MRD-JOURNAL-D-21-00045.1, 2022.

Caloiero, T., Coscarelli, R., and Gaudio, R.: Spatial and temporal variability of daily precipitation concentration in the Sardinia region (Italy), International Journal of Climatology, 39, 5006–5021, https://doi.org/10.1002/JOC.6123, 2019.

https://doi.org/10.5194/nhess-2023-120
Preprint. Discussion started: 8 August 2023

Cavallo, E. and Noy, I.: The Economics of Natural Disasters A Survey, 2010.

Chen, T. and Guestrin, C.: XGBoost: A Scalable Tree Boosting System, Proceedings of the ACM SIGKDD International Conference on Knowledge Discovery and Data Mining, 13-17-August-2016, 785–794, https://doi.org/10.1145/2939672.2939785, 2016.

Chen, T., He, T., and Benesty, M.: XGBoost : eXtreme Gradient Boosting, R package version 0.71-2, 1–4, 2018.

Criss, R. E. and Shock, E. L.: Flood enhancement through flood control, Geology, 29, 875, https://doi.org/10.1130/0091-7613(2001)029<0875:FETFC>2.0.CO;2, 2001.

Delalay, M., Ziegler, A. D., Shrestha, M. S., Wasson, R. J., Sudmeier-Rieux, K., McAdoo, B. G., and Kochhar, I.: Towards improved flood disaster governance in Nepal: A case study in Sindhupalchok District, International Journal of Disaster Risk Reduction, 31, 354–366, https://doi.org/10.1016/j.ijdrr.2018.05.025, 2018.

Deroliya, P., Ghosh, M., Mohanty, M. P., Ghosh, S., Rao, K. H. V. D., and Karmakar, S.: A novel flood risk mapping approach with machine learning considering geomorphic and socio-economic vulnerability dimensions, Science of the Total Environment, 851, https://doi.org/10.1016/j.scitotenv.2022.158002, 2022.

Diehl, R. M., Gourevitch, J. D., Drago, S., and Wemple, B. C.: Improving flood hazard datasets using a low-complexity, probabilistic floodplain mapping approach, PLoS One, 16, https://doi.org/10.1371/journal.pone.0248683, 2021.

Dingle, E. H., Creed, M. J., Sinclair, H. D., Gautam, D., Gourmelen, N., Borthwick, A. G. L., and Attal, M.: Dynamic flood topographies in the Terai region of Nepal, Earth Surf Process Landf, 45, 3092–3102, https://doi.org/10.1002/esp.4953, 2020a.

Dingle, E. H., Creed, M. J., Sinclair, H. D., Gautam, D., Gourmelen, N., Borthwick, A. G. L., and Attal, M.: Dynamic flood topographies in the Terai region of Nepal, Earth Surf Process Landf, 45, 3092–3102, https://doi.org/10.1002/esp.4953, 2020b.

Dottori, F., Alfieri, L., Bianchi, A., Skoien, J., and Salamon, P.: A new dataset of river flood hazard maps for Europe and the Mediterranean Basin, Earth Syst Sci Data, 14, 1549–1569, https://doi.org/10.5194/essd-14-1549-2022, 2022.

Fischer, M., Brettin, J., Roessner, S., Walz, A., Fort, M., and Korup, O.: Rare flood scenarios for a rapidly growing high-mountain city: Pokhara, Nepal, n.d.

Haag, I., Jones, P. D., and Samimi, C.: Central Asia's Changing Climate: How Temperature and Precipitation Have Changed across Time, Space, and Altitude, Climate 2019, Vol. 7, Page 123, 7, 123, https://doi.org/10.3390/CLI7100123, 2019.

Hawker, L., Rougier, J., Neal, J., Bates, P., Archer, L., and Yamazaki, D.: Implications of Simulating Global Digital Elevation Models for Flood Inundation Studies, Water Resour Res, 54, 7910–7928, https://doi.org/10.1029/2018WR023279, 2018.

ICIMOD: Glacial Lakes and Glacial Lake Outburst Floods in Nepal, 2011.

Jongejan, R. B. and Maaskant, B.: Quantifying flood risks in the Netherlands, Risk Analysis, 35, 252–264, https://doi.org/10.1111/risa.12285, 2015.

Kafle, K. R., Khanal, S. N., and Dahal, R. K.: Consequences of Koshi flood 2008 in terms of sedimentation characteristics and agricultural practices, Geoenvironmental Disasters, 4, 1–13, https://doi.org/10.1186/S40677-017-0069-X/FIGURES/15, 2017.

Karki, R., ul Hasson, S., Schickhoff, U., Scholten, T., and Böhner, J.: Rising Precipitation Extremes across Nepal, Climate 2017, Vol. 5, Page 4, 5, 4, https://doi.org/10.3390/CLI5010004, 2017.

Kayastha, R. B. and Kayastha, R.: Glacio-Hydrological Degree-Day Model (GDM) Useful for the Himalayan River Basins, Himalayan Weather and Climate and their Impact on the Environment, 379–398, https://doi.org/10.1007/978-3-030-29684-1_19, 2019.

Kiran S, Yogacharya, and Gautam, D. K.: Floods in Nepal: Genesis, Magnitude, Frequencyand Consequences, in: Proc. of the International Conference on Hydrology and Climate Change in Mountainous Areas, https://doi.org/10.13140/RG.2.1.2376.8489, 2008.

Kirschbaum, D., Kapnick, S. B., Stanley, T., and Pascale, S.: Changes in Extreme Precipitation and Landslides Over High Mountain Asia, Geophys Res Lett, 47, https://doi.org/10.1029/2019GL085347, 2020.

Lane, S. N., Tayefi, V., Reid, S. C., Yu, D., and Hardy, R. J.: Interactions between sediment delivery, channel change, climate change and flood risk in a temperate upland environment, Earth Surf Process Landf, 32, 429–446, https://doi.org/10.1002/esp.1404, 2007.

Lindersson, S., Brandimarte, L., Märd, J., and di Baldassarre, G.: Global riverine flood risk - How do hydrogeomorphic floodplain maps compare to flood hazard maps?, Natural Hazards and Earth System Sciences, 21, 2921–2948, https://doi.org/10.5194/nhess-21-2921-2021, 2021.

Marston, R., Kleinman, J., and Miller, M.: Geomorphic and forest cover controls on monsoon flooding, central Nepal Himalaya, Mt Res Dev, 16, 257–264, https://doi.org/10.2307/3673948, 1996.

Martin-Vide, J.: Spatial distribution of a daily precipitation concentration index in peninsular Spain, International Journal of Climatology, 24, 959–971, https://doi.org/10.1002/JOC.1030, 2004.

Mathers, C., Stevens, G., Ho, J., Ma Fat, D., Retno Mahanani, W., Andreev, K., Bassani, D., Black, B., Boerma, T., Boucher, P., Bray, F., Burton, T., Campbell, H., Chou, D., Cibulskis, R., Cousens, S., Ferlay, J., Gacic-Dobo, M., Garfield, R., Gemmill, A., Gerland, P., Ghys, P., Glaziou, P., Gu, D., Hill, K., Iaych, K., Inoue, M., Jakob, R., Jamison, D., Jha, P., Johnson, H., Lawn, J., Li, N., Liu, L., Lozano, R., Mahi, M., Murray, C., Newman, L., Oestergaard, M., Parkin, M., Peden, M., Pelletier, F., Rehm, J., Rudan, I., Say, L., Simons, E., Sismanidis, C., Spoorenberg, T., Stanecki, K., Stover, J., Strebel, P., Suzuki, E., Toroyan, T., Vos, T., Wardlaw, T., White, R., Wilmoth, J., and You, D.: WHO methods and data sources for global burden of disease estimates 2000-2011, 2013.

Meyer, V., Becker, N., Markantonis, V., Schwarze, R., Van Den Bergh, J. C. J. M., Bouwer, L. M., Bubeck, P., Ciavola, P., Genovese, E., Green, C., Hallegatte, S., Kreibich, H., Lequeux, Q., Logar, I., Papyrakis, E., Pfurtscheller, C., Poussin, J., Przyluski, V., Thieken, A. H., and Viavattene, C.: Review article: Assessing the costs of natural hazards-state of the art and knowledge gaps, https://doi.org/10.5194/nhess-13-1351-2013, 2013.

Mohanty, M. P. and Simonovic, S. P.: A Comprehensive Approach for Floodplain Mapping through Identification of Hazard Using Publicly Available Data Sets over Canada, Water (Switzerland), 14, https://doi.org/10.3390/w14142280, 2022.

Monjo, R.: Measure of rainfall time structure using the dimensionless n-index, Clim Res, 67, 71–86, https://doi.org/10.3354/cr01359, 2016.

Monjo, R. and Martin-Vide, J.: Daily precipitation concentration around the world according to several indices, International Journal of Climatology, 36, 3828–3838, https://doi.org/10.1002/JOC.4596, 2016.

Mosavi, A., Ozturk, P., and Chau, K. W.: Flood prediction using machine learning models: Literature review, https://doi.org/10.3390/w10111536, 27 October 2018.

Neuhold, C., Stanzel, P., and Nachtnebel, H. P.: Incorporating river morphological changes to flood risk assessment: Uncertainties, methodology and application, Natural Hazards and Earth System Science, 9, 789–799, https://doi.org/10.5194/nhess-9-789-2009, 2009.

Noy, I.: Prepared for the 2015 Global Assessment Report on Disaster Risk Reduction A NON-MONETARY GLOBAL MEASURE OF THE DIRECT IMPACT OF NATURAL DISASTERS, 2014.

Noy, I.: Comparing the direct human impact of natural disasters for two cases in 2011: The Christchurch earthquake and the Bangkok flood, International Journal of Disaster Risk Reduction, 13, 61–65, https://doi.org/10.1016/j.ijdrr.2015.03.009, 2015.

Noy, I.: A Global Comprehensive Measure of the Impact of Natural Hazards and Disasters, Glob Policy, 7, 56–65, https://doi.org/10.1111/1758-5899.12272, 2016a.

Noy, I.: Natural disasters in the Pacific Island Countries: new measurements of impacts, Natural Hazards, 84, 7–18, https://doi.org/10.1007/s11069-015-1957-6, 2016b.

Pangali Sharma, T. P., Zhang, J., Koju, U. A., Zhang, S., Bai, Y., and Suwal, M. K.: Review of flood disaster studies in Nepal: A remote sensing perspective, https://doi.org/10.1016/j.ijdrr.2018.11.022, 1 March 2019.

Pervin, I. A., Rahman, S. M. M., Nepal, M., Haque, A. K. E., Karim, H., and Dhakal, G.: Adapting to urban flooding: A case of two cities in South Asia, Water Policy, 22, 162–188, https://doi.org/10.2166/wp.2019.174, 2020.

Piacentini, T., Carabella, C., Boccabella, F., Ferrante, S., Gregori, C., Mancinelli, V., Pacione, A., Pagliani, T., and Miccadei, E.: Geomorphology-Based analysis of flood critical areas in small hilly catchments for civil protection purposes and earlywarning systems: The case of the feltrino stream and the Lanciano Urban Area (Abruzzo, Central Italy), Water (Switzerland), 12, https://doi.org/10.3390/w12082228, 2020.

Pinter, N., Jemberie, A. A., Remo, J. W. F., Heine, R. A., and Ickes, B. S.: Flood trends and river engineering on the Mississippi River system, Geophys. Res. Lett, 35, 23404, https://doi.org/10.1029/2008GL035987, 2008.

Rentschler, J., Salhab, M., and Jafino, B. A.: Flood exposure and poverty in 188 countries, Nat Commun, 13, https://doi.org/10.1038/s41467-022-30727-4, 2022.

Samela, C., Troy, T. J., and Manfreda, S.: Geomorphic classifiers for flood-prone areas delineation for data-scarce environments, Adv Water Resour, 102, 13–28, https://doi.org/10.1016/j.advwatres.2017.01.007, 2017.

Sangüesa, C., Pizarro, R., Ibañez, A., Pino, J., Rivera, D., García-Chevesich, P., and Ingram, B.: Spatial and temporal analysis of rainfall concentration using the Gini Index and PCI, Water (Switzerland), 10, https://doi.org/10.3390/w10020112, 2018.

Sanyal, J. and Lu, X. X.: Application of Remote Sensing in Flood Management with Special Reference to Monsoon Asia: A Review, Natural Hazards, 283–301 pp., 2004.

Serrano-Notivoli, R., Martín-Vide, J., Saz, M. A., Longares, L. A., Beguería, S., Sarricolea, P., Meseguer-Ruiz, O., and de Luis, M.: Spatio-temporal variability of daily precipitation concentration in Spain based on a high-resolution gridded data set, International Journal of Climatology, 38, e518–e530, https://doi.org/10.1002/JOC.5387, 2018.

Sharma, P. p. T., Zhang, J., Koju, A. U., Zhang, S., Bai, Y., and Suwal, K. M.: International Journal of Disaster Risk Reduction Review of fl ood disaster studies in Nepal : A remote sensing perspective Til Prasad Pangali Sharma, International Journal of Disaster Risk Reduction, 34, 18–27, 2019.

High Mountain Asia 8-meter DEM Mosaics Derived from Optical Imagery, Version 1 | National Snow and Ice Data Center: https://nsidc.org/data/hma_dem8m_mos/versions/1, last access: 20 March 2023.

High Mountain Asia 8-meter DEMs Derived from Along-track Optical Imagery, Version 1 | National Snow and Ice Data Center: https://nsidc.org/data/hma_dem8m_at/versions/1, last access: 20 March 2023.

High Mountain Asia 8-meter DEMs Derived from Cross-track Optical Imagery, Version 1 | National Snow and Ice Data Center: https://nsidc.org/data/hma_dem8m_ct/versions/1, last access: 20 March 2023.

Shrestha, A. B. and Aryal, R.: Climate change in Nepal and its impact on Himalayan glaciers, Reg Environ Change, 11, 65–77, https://doi.org/10.1007/s10113-010-0174-9, 2011.

Shrestha, A. B., Eriksson, M., Mool, P., Ghimire, P., Mishra, B., and Khanal, N. R.: Glacial lake outburst flood risk assessment of Sun Koshi basin, Nepal, Geomatics, Natural Hazards and Risk, 1, 157–169, https://doi.org/10.1080/19475701003668968, 2010.

Simonovic, S. P., Karmakar, S., Cheng, Z., Kansal, M. L., and Singh, S.: Flood Management Issues in Hilly Regions of Uttarakhand (India) under Changing Climatic Conditions, Water 2022, Vol. 14, Page 1879, 14, 1879, https://doi.org/10.3390/W14121879, 2022.

Slater, L. J., Singer, M. B., and Kirchner, J. W.: Hydrologic versus geomorphic drivers of trends in flood hazard, Geophys Res Lett, 42, 370–376, https://doi.org/10.1002/2014GL062482, 2015a.

Slater, L. J., Singer, M. B., and Kirchner, J. W.: Hydrologic versus geomorphic drivers of trends in flood hazard, Geophys Res Lett, 42, 370–376, https://doi.org/10.1002/2014GL062482, 2015b.

Slater, L. J., Khouakhi, A., and Wilby, R. L.: River channel conveyance capacity adjusts to modes of climate variability, Sci Rep, 9, 1–10, https://doi.org/10.1038/s41598-019-48782-1, 2019.

Sofia, G. and Nikolopoulos, E. I.: Floods and rivers: a circular causality perspective, Sci Rep, 10, https://doi.org/10.1038/s41598-020-61533-x, 2020.

Sofia, G., Tarolli, P., Cazorzi, F., and Dalla Fontana, G.: Downstream hydraulic geometry relationships: Gathering reference reach-scale width values from LiDAR, Geomorphology, 250, 236–248, https://doi.org/10.1016/j.geomorph.2015.09.002, 2015.

Sofia, G., Roder, G., Dalla Fontana, G., and Tarolli, P.: Flood dynamics in urbanised landscapes: 100 years of climate and humans' interaction, Sci Rep, 7, 1–12, https://doi.org/10.1038/srep40527, 2017a.

https://doi.org/10.5194/nhess-2023-120
Preprint. Discussion started: 8 August 2023

Sofia, G., di Stefano, C., Ferro, V., and Tarolli, P.: Morphological Similarity of Channels: From Linear Erosional Features (Rill, Gully) to Alpine Rivers, Land Degrad Dev, 28, 1717–1728, https://doi.org/10.1002/ldr.2703, 2017b.

Sofia, G., di Stefano, C., Ferro, V., and Tarolli, P.: Morphological Similarity of Channels: From Linear Erosional Features (Rill, Gully) to Alpine Rivers, Land Degrad Dev, 28, 1717–1728, https://doi.org/10.1002/ldr.2703, 2017c.

Stover, S. C. and Montgomery, D. R.: Channel change and flooding, Skokomish River, Washington, J Hydrol (Amst), 243, 272–286, https://doi.org/10.1016/S0022-1694(00)00421-2, 2001.

Subba, S., Ma, Y., and Ma, W.: Spatial and Temporal Analysis of Precipitation Extremities of Eastern Nepal in the Last Two Decades (1997–2016), Journal of Geophysical Research: Atmospheres, 124, 7523–7539, https://doi.org/10.1029/2019JD030639, 2019.

Talchabhadel, R., Karki, R., Thapa, B. R., Maharjan, M., and Parajuli, B.: Spatio-temporal variability of extreme precipitation in Nepal, International Journal of Climatology, 38, 4296–4313, https://doi.org/10.1002/JOC.5669, 2018.

Torti, J. M. I.: Floods in Southeast Asia: A health priority, J Glob Health, 2, https://doi.org/10.7189/jogh.02.020304, 2012.

Tuladhar, D., Dewan, A., Kuhn, M., and Corner, R. J.: Spatio-temporal rainfall variability in the Himalayan mountain catchment of the Bagmati River in Nepal., Theor Appl Climatol, 139, 599–615, https://doi.org/10.1007/S00704-019-02985-8, 2020.

WHO: GlobalDALYmethodsJapan_2011_WHO, World Health Organization, 4, 2014.

Yang, C. R. and Tsai, C. T.: Development of a GIS-based flood information system for floodplain modeling and damage calculation, J Am Water Resour Assoc, 36, 567–577, https://doi.org/10.1111/j.1752-1688.2000.tb04287.x, 2000.

Zheng, G., Allen, S. K., Bao, A., Ballesteros-Cánovas, J. A., Huss, M., Zhang, G., Li, J., Yuan, Y., Jiang, L., Yu, T., Chen, W., and Stoffel, M.: Increasing risk of glacial lake outburst floods from future Third Pole deglaciation, Nat Clim Chang, 11, 411–417, https://doi.org/10.1038/s41558-021-01028-3, 2021.

Zheng, X., Maidment, D. R., Tarboton, D. G., Liu, Y. Y., and Passalacqua, P.: GeoFlood: Large-Scale Flood Inundation Mapping Based on High-Resolution Terrain Analysis, Water Resour Res, 54, 10,013-10,033, https://doi.org/10.1029/2018WR023457, 2018.